Reinforcement Load and Compression of Reinforced Soil Mass under Surcharge Loading

Huabei Liu, M.ASCE[1]

Abstract: Reinforced soil composites and mechanically stabilized earth (MSE) walls are frequently employed to carry large surcharge or footing loads. For the safety and serviceability of these reinforced soil structures, it is necessary to analyze the reinforcement load and compression of reinforced soil mass subjected to surcharge loading. In the research reported in this paper, an analytical method proposed by the writer was extended to meet these needs. The extended analytical method explicitly considers soil nonlinearity, soil dilatancy, soil-reinforcement interaction, and end restrictions of reinforced soil mass. Both plane-strain and triaxial stress states can be considered in the method. The applicability of the method for reinforcement load was validated against eight large-scale tests of reinforced soil mass or MSE walls, and the method for reinforced soil compression was validated against two large-scale tests. The compressions of four reinforced soil minipiers under surcharge loading were also predicted. The proposed method has the capacity to unify the analyses of reinforcement load and compression of a reinforced soil mass under low to medium surcharge loading. Some issues in the application of the proposed method are also discussed. **DOI: 10.1061/(ASCE)GT.1943-5606.0001300.**

Author keywords: Reinforcement load; Compression; Analytical method; Reinforced soil mass; Surcharge loading.

Introduction

Reinforced soil composites and mechanically stabilized earth (MSE) walls are frequently employed to carry large surcharge or footing loads. Among the applications, geosynthetic-reinforced soil (GRS) bridge abutments and piers are reliable and cost-effective for critical applications (Abu-Hejleh et al. 2002; Adams et al. 2002, 2007, 2011; Uchimura et al. 2003; Nicks et al. 2013). Design of these reinforced soil structures requires an analysis of the reinforcement load under external loading. For the application of bridge abutments and piers, it is also necessary to estimate the compression (Adams et al. 2011).

Conventional design of MSE walls generally utilizes earth pressure theories or limit equilibrium to calculate the reinforcement load (e.g., Leshchinsky and Boedeker 1989; Berg et al. 2009). Full mobilization of soil strength is assumed while analyzing the reinforcement loads of GRS retaining walls. However, as discussed in Liu and Won (2014), the mobilized soil strength and reinforcement load can vary considerably in different geosynthetic-reinforced MSE walls subjected to different levels of surcharge loading. In the design of a GRS integral bridge system (IBS), Adams et al. (2011) proposed a semiempirical approach to calculate the required reinforcement strength in GRS bridge abutments, which is not necessarily the actual mobilized reinforcement load under surcharge loading.

Nonconventional methods have also been proposed to analyze the reinforcement loads of MSE walls. Among the available methods, the methods by Juran and Chen (1989), Juran et al. (1990), Abramento and Whittle (1993), Ehrlich and Mitchell (1994), and Liu and Won (2014) explicitly consider soil-reinforcement interaction, some also take into account the nonlinear behavior (Juran and Chen 1989; Juran et al. 1990; Ehrlich and Mitchell 1994; Liu and Won 2014) and stress-dilatancy (Liu and Won 2014) of soil. The *k*-stiffness method proposed in Allen et al. (2004) and Bathurst et al. (2008) is an empirical method. It also takes into account the effect of reinforcement stiffness but the soil strength instead of soil stiffness is used as a parameter in this method.

To estimate the compression of reinforced soil mass, Adams et al. (2011) suggests that minipier test be conducted to extract the information. Recently, Hoffman and Wu (2014) proposed an analytical method to estimate the compression of GRS piers with closely spaced reinforcement layers. The method takes into account the soil-reinforcement interaction but the degradation of soil stiffness with loading is not considered. It also does not consider the effect of end restriction on the compression.

In the research reported in this paper, the analytical method proposed by Liu and Won (2014), which considers soil-reinforcement interaction, soil nonlinearity, and soil dilatancy, was extended to analyze for the reinforcement load and average compression of reinforced soil mass under surcharge loading. The method was validated by a series of large-scale tests and it was used to predict the compressions of four GRS minipiers subjected to surcharge loading (Nicks et al. 2013).

Analytical Method

Analysis of Reinforcement Load and Soil Strain

In the analytical method, it is assumed that the reinforced soil mass is constructed over a stiff foundation, and the vertical stress σ_z and lateral stress σ_l are the major and minor principal stresses, respectively. Vertical stress is $\sigma_z = \gamma z + \Delta\sigma_z$, where γ is the unit weight of soil, z is the depth, and $\Delta\sigma_z$ is the additional stress induced by surcharge loading. With uniform surcharge q, $\Delta\sigma_z = q$; otherwise it can be calculated using available methods (Berg et al. 2009).

In Liu and Won (2014), plane-strain condition of soil is assumed. This assumption is applicable to most MSE walls and many

[1]Professor, School of Civil Engineering and Mechanics, Huazhong Univ. of Science and Technology, 1037 Luoyu Rd., Wuhan, Hubei 430074, China. E-mail: hbliu@hust.edu.cn

Note. This manuscript was submitted on July 13, 2014; approved on December 30, 2014; published online on February 9, 2015. Discussion period open until July 9, 2015; separate discussions must be submitted for individual papers. This paper is part of the ***Journal of Geotechnical and Geoenvironmental Engineering***, © ASCE, ISSN 1090-0241/04015017 (10)/$25.00.

reinforced soil abutments but for many reinforced soil piers (Nicks et al. 2013) the lateral deformations of soil in two orthogonal directions are not very different, and the assumption of triaxial stress state may be appropriate.

In accordance with Liu and Won (2014), the incremental stress-strain relationship of soil in triaxial or plane-strain stress state may be expressed as

$$\Delta\sigma_z - \Delta\sigma_l = C_t \Delta\varepsilon_z \tag{1}$$

where

$$C_t = k p_a \left(\frac{\sigma_l}{p_a}\right)^n \left[1 - R_f \frac{(\sigma_z - \sigma_l)(1-\sin\phi)}{2c\cos\phi + 2\sigma_l \sin\phi}\right]^2 \tag{2}$$

where $\Delta\sigma_z$, $\Delta\sigma_l$, and $\Delta\varepsilon_z$ are increments of vertical soil stress, lateral soil stress, and vertical soil strain, respectively. In the triaxial stress state, C_t is the tangent modulus of soil E_t (Duncan et al. 1980) but it is generally larger than E_t in the plane-strain condition, depending on soil dilatancy (Hatami and Bathurst 2006). k is the modulus number, n is the modulus exponent, R_f is the failure ratio of the soil, and p_a is the atmospheric pressure. c and ϕ are the cohesion and internal angle of friction of soil, respectively.

The deformation of soil is assumed to be inelastic in accordance with the stress-dilatancy relationship of Rowe (1962). Neglecting elastic deformation and assuming a plane-strain condition, the stress-dilatancy relationship can be written in incremental form as (Wood 1990)

$$\frac{\sigma_z}{\sigma_l}\left(\frac{\Delta\varepsilon_z}{\Delta\varepsilon_l}\right) = K \tag{3}$$

where K is the Rowe (1962) dilatancy constant, and ε_l = magnitude of lateral soil strain. In the triaxial stress state, the stress dilatancy relationship can be expressed as (Wood 1990)

$$\frac{\sigma_z}{\sigma_l}\left(\frac{\Delta\varepsilon_z}{\Delta\varepsilon_l}\right) = 2K \tag{4}$$

The proposed method calculates the maximum reinforcement load in one reinforcement layer and at that location, the lateral strains of soil and reinforcement are compactible (Liu and Won 2014). Accordingly the lateral soil stress σ_l can be related to the reinforcement load per meter, T, through Eq. (5)

$$\sigma_l = T/S_v + \sigma_{l0} = J\varepsilon_l/S_v + \sigma_{l0} \tag{5}$$

or in incremental form

$$\Delta\sigma_l = J\Delta\varepsilon_l/S_v \tag{6}$$

where σ_{l0} = lateral stress applied externally on the reinforced soil mass; J = reinforcement stiffness; and S_v = vertical reinforcement spacing. Combination of Eqs. (3) and (4) and (5) and (6) leads to

$$\Delta T = J\Delta\sigma_z / \left[K\left(\frac{\sigma_l}{\sigma_z}\right)C_t + \frac{J}{S_v}\right] \tag{7a}$$

$$\Delta T = J\Delta\sigma_z / \left[2K\left(\frac{\sigma_l}{\sigma_z}\right)C_t + \frac{J}{S_v}\right] \tag{7b}$$

Eq. (7a) can be used to calculate the reinforcement load with the assumption of plane-strain condition, while Eq. (7b) is for the triaxial stress state. From Eqs. (3) and (4), the vertical soil strain is written as Eqs. (8a) or (8b) for the plane-strain or triaxial stress condition, respectively

$$\Delta\varepsilon_z = K\left(\frac{\sigma_l}{\sigma_z}\right)\Delta\varepsilon_l \tag{8a}$$

$$\Delta\varepsilon_z = 2K\left(\frac{\sigma_l}{\sigma_z}\right)\Delta\varepsilon_l \tag{8b}$$

Average Compression of Reinforced Soil Mass

Eqs. (8a) and (8b) can be applied to calculate the compression of reinforced soil mass under surcharge loading, provided that the lateral soil strain is only restricted by the reinforcement. However, large-scale or full-scale tests have shown that foundation restriction results in a smaller reinforcement load and soil strain close to the base (e.g., Walters 2004; Elton and Patawaran 2004; Allen et al. 2004; Wu et al. 2013). For a reinforced soil bridge pier or abutment, the bridge beam also restrains the lateral deformation in the soil and reinforcement (Adams et al. 2002; Elton and Patawaran 2004; Wu et al. 2013).

The restrictions at the two ends of reinforced soil mass not only restrain the lateral soil deformation; they also reduce the vertical soil strain. From the viewpoint of soil stress and deformation, the restriction effectually increases the confining pressure on the soil and under the same vertical stress, the soil stiffness would be larger and the vertical soil strain would be smaller, as can be seen in Eq. (2).

In order to consider the effect of restriction on the compression of reinforced soil mass, the reinforcement layers close to the ends may be assigned larger stiffness values. The virtual stiffness plays the role of end restriction in the analytical method, which improves the confining pressure on the soil and enhances soil stiffness, as can be seen in Eqs. (5) and (6).

Under the plane-strain condition, the increment of lateral soil strain can be written as Eq. (9) according to Eqs. (7a) and (7b)

$$\Delta\varepsilon_l = \Delta\sigma_z / \left[K\left(\frac{J\varepsilon_l}{S_v\sigma_z}\right)C_t + \frac{J}{S_v}\right] \tag{9}$$

where it is assumed that the reinforcement stiffness is a constant. Integration of Eq. (9) leads to

$$\varepsilon_l = \frac{S_v}{J}\int_0^{\sigma_z} \frac{\sigma_z}{(K\varepsilon_l C_t + \sigma_z)} d\sigma_z \tag{10}$$

Let the lateral soil strain with end restriction be ε_l^r; it can expressed as

$$\varepsilon_l^r = \frac{S_v}{J_v}\int_0^{\sigma_z} \frac{\sigma_z}{(K\varepsilon_l^r C_t^r + \sigma_z)} d\sigma_z \tag{11}$$

where J_v is the virtual reinforcement stiffness to simulate the effect of end restriction. C_t^r is the tangent soil modulus corresponding to ε_l^r. Eqs. (10) and (11) results in Eq. (12)

$$\frac{\varepsilon_l^r}{\varepsilon_l} = \frac{J}{J_v}\int_0^{\sigma_z} \frac{K\varepsilon_l C_t + \sigma_z}{K\varepsilon_l^r C_t^r + \sigma_z} d\sigma_z \tag{12}$$

Eq. (12) cannot be solved analytically. However, under the same vertical stress σ_z, the end-restraint leads to larger C_t^r than C_t, but the

J. Geotech. Geoenviron. Eng., 2015, 141(6): 04015017

lateral soil strain ε_l^r is smaller than ε_l. The relationship in Eq. (12) depends on the ratio between $\varepsilon_l^r C_l^r$ and $\varepsilon_l C_l$. This ratio may not be a constant but a function of stress level and soil dilatancy. However, it is not expected to be significantly different from 1.0. At this stage, the ratio of lateral soil strains is conveniently approximated as

$$\frac{\varepsilon_l^r}{\varepsilon_l} \approx \frac{J}{J_v} \tag{13}$$

The same ratio can be obtained with the assumption of a triaxial stress state.

With Eq. (13), the influence of end restriction on the compression of reinforced soil mass can be simulated, provided that the distribution of lateral reinforcement strain in the reinforced soil mass under loading is known. Elton and Patawaran (2004) reported that the lateral reinforcement strain in a reinforced soil mass subjected to surcharge loading could be approximated by a trapezoid. The strain was zero at the end and increased linearly to $0.2H$, where H is the height of the reinforced soil mass. Allen et al. (2004) and Bathurst et al. (2008) also proposed a trapezoidal distribution of reinforcement strain for MSE walls. As the proposed method targets the compression under surcharge loading, the empirical distribution proposed by Elton and Patawaran (2004) is employed.

With the vertical soil strain ε_z^i at each layer of reinforcement, the average compression ε_c of a reinforced soil mass can be approximated by the weighted average value

$$\varepsilon_c = \frac{\sum(\varepsilon_z^i S_v^i)}{\sum S_v^i} \tag{14}$$

where S_v^i = reinforcement spacing, which may not be uniform in the reinforced soil mass.

Effect of Soil Compaction

Soil compaction induces locked-in lateral stress in the soil and residual load in the reinforcement layers (Bathurst et al. 2009; Ehrlich et al. 2012), but the effect on the reinforcement load is erased with a certain level of surcharge loading, depending on the compaction method (Bathurst et al. 2009; Liu and Won 2014). The method proposed in this paper targets the behavior under surcharge loading, hence the effect of soil compaction is not considered. This assumption would underestimate the reinforcement load but overestimate the vertical strain at small surcharge loading.

Identifications of Model Parameters

Implementation and application of the proposed method requires the input of the height of reinforced soil mass, locations of reinforcement layers, surface surcharge q, soil properties, and reinforcement stiffness. Soil properties consist of soil strength (c and ϕ), soil unit weight γ, and deformation properties of soil (k, n, R_f, and K).

The soil parameters k, n, R_f, c, and ϕ are the conventional hyperbolic model constants for soil if the behavior of a reinforced soil pier is analyzed, and they can be obtained from two triaxial compression tests (Duncan et al. 1980). If reinforced soil retaining walls are analyzed, the parameters may be curve-fitted from results of two plane-strain compression tests; however, if the tests are not available, the plane-strain strength can be estimated from the triaxial strength (e.g., Georgiadis et al. 2004), while the stiffness parameters can conservatively assume the hyperbolic parameters fitting triaxial compression test results. If the variation of soil stress in the composite is large, the dependence of friction angle ϕ on the confining pressure can be considered by $\phi = \phi_0 - \Delta\phi \log(\sigma_l / p_a)$, where ϕ_0 is the friction angle at the reference pressure p_a, and $\Delta\phi$ is the decrease of friction angle with confining pressure (Duncan et al. 1980). The Rowe (1962) dilatancy constant K can be estimated by $K = (1 + \sin\phi_{cr})/(1 - \sin\phi_{cr})$ or $K = (1 + \sin\phi)(1 - \sin\psi)/[(1 - \sin\phi)(1 + \sin\psi)]$ (Wood 1990), where ϕ_{cr} is the residual friction angle of soil, and ψ is the angle of dilatancy.

The reinforcement stiffness may be obtained from a uniaxial tension test of the geosynthetics if the short-term behavior after loading is the interest. However, if the long-term reinforcement load and reinforced soil deformation are to be obtained, the long-term stiffness may be interpreted from the isochrones of the geosynthetics (Allen et al. 2004; Liu and Won 2014). The values of the virtual reinforcement stiffness J_v for the reinforcement layers close to the ends can be estimated by Eq. (13) using the assumed trapezoidal distribution of reinforcement strains in the reinforced soil mass (Elton and Patawaran 2004).

Large-Scale Tests of Reinforced Soil Masses or MSE Walls

Large-scale tests on two GRS composites, five reinforced soil piers, two reinforced soil abutments, and three MSE walls were analyzed, among which seven tests were carried out at the Turner-Fairbank Highway Research Center (TFHRC), and the term Turner-Fairbank (TF) is assigned for their designations. These tests are summarized in Table 1, the analysis conditions are given in Table 2, while the soil parameters are shown in Table 3.

Turner-Fairbank Geosynthetic-Reinforced Soil Composites

This section discusses TF geosynthetic-reinforced soil composites (GRSCs) as per Wu et al. (2013). Two large-scale tests on GRS composites by Wu et al. (2013) were analyzed for reinforcement load and compression under four levels of surcharge loading. The reinforcement loads estimated in the research reported in this paper were also the maximum in the reinforced soil composites. The composites were 2-m high and 1.35-m wide, and tested in plane-strain conditions. Woven polypropylene (PP) geotextile was used as the reinforcement, the stiffness of which in standard uniaxial tension test was approximately 1,000 kN/m at small strain ($\varepsilon < 2\%$). The reinforcement spacing was 0.2 and 0.4 m for GRSC I and II, respectively. The fill material was a well-graded gravel with silt (GW-GM) compacted to a dry unit weight of 24 kN/m^3. The moist unit weight in the test was 25 kN/m^3. In the loading tests, GRS composites were subjected to a lateral confining pressure of 34 kPa ($\sigma_{l0} = 34$ kPa).

Drained triaxial tests were carried out on the soil by Wu et al. (2013). The triaxial friction angle was estimated assuming no cohesion. As discussed in Liu and Won (2014), the plane-strain friction angle was estimated as $\phi_{ps} = 60° - 15.45 \log(\sigma_3 / p_a)$ according to the Matsuoka-Nakai failure criterion (Georgiadis et al. 2004). The angle of dilatancy was reported to be 17.5°, based on which the dilatancy constant K was calculated. The soil deformation constants were curve-fitted from the triaxial test results, but in accordance with Wu et al. (2014), the modulus number k was increased to 1,268 to take into account the plane-strain condition.

Old TF Pier

This section discusses an old TF pier as per Wu et al. (2001). The full-scale test was conducted at the TFHRC. The height of the test

Table 1. Parameters of Reinforced Soil Masses or MSE Walls

Reinforced soil mass or MSE wall	Height (m)	Facing	Backfill	RF[a] spacing (m)	RF type	RF stiffness (kN/m)
TF[b] GRSC I[c]	2	None	Gravel	0.2	Polypropylene geotextile	1,000[d]
TF GRSC II[c]	2	None	Gravel	0.4	Polypropylene geotextile	1,000[d]
Old TF pier[e]	5.4	Block	Gravel	0.2	Polypropylene geotextile	1,200, 960[f]
National Cooperative Highway Research Program abutment[g]	4.65	Block	Silty sand	0.1, 0.2	Polypropylene geotextile	400[h]
Japanese abutment[i]	5	Wrapped around	Gravel	0.3	PVA geogrid	1,000[j]
Shored MSE wall[k]	5.5	Welded wire	Sand	0.23, 0.46	High-density polypropylene geogrid	1,300[l]
French MSE wall[m]	4.35	Block	Sand	0.29,0.58,1.16	Woven geotextile	390[n]
Royal Military College MSE wall[o]	3.6	Wrapped around	Sand	0.6	Wire-welded mesh	3,100[p]
New TF Pier 6[q]	1.95	Block	Gravel	0.195	Polypropylene geotextile	1,000[r]
New TF Pier 9[q]	1.95	Block	Gravel	0.39	Polypropylene geotextile	1,000[r]
New TF Pier 12[q]	1.95	Block	Gravel	0.095	Polypropylene geotextile	300[r]
New TF Pier 14[q]	1.995	Block	Gravel	0.285	Polypropylene geotextile	510[r]

[a]Reinforcement.
[b]Turner-Fairbank.
[c]Wu et al. (2013).
[d]Stiffness provided in Wu et al. (2013).
[e]Wu et al. (2001).
[f]Test data from Helwany et al. (2007).
[g]Wu et al. (2006a).
[h]Test data from Helwany et al. (2007).
[i]Uchimura et al. (1996).
[j]Test data from Kongkitkul et al. (2007).
[k]Morrison et al. (2006).
[l]Stiffness provided in Morrison et al. (2006).
[m]Arab et al. (2001).
[n]Test data from Arab et al. (2001).
[o]Walters (2004).
[p]Stiffness provided in Walters (2004).
[q]Nicks et al. (2013).
[r]Stiffness interpreted from Nicks et al. (2013).

Table 2. Analysis Conditions for the Reinforced Soil Masses or MSE Walls

Reinforced soil mass or MSE wall	Approximated stress condition	Analyzed RF layer location from top (m)	Load type	Analyzed pressure (kPa)
Turner-Fairbank GRSC I	Plane strain	0.6	Uniform pressure	200, 400, 600, and 800
Turner-Fairbank GRSC II	Plane strain	0.4	Uniform pressure	100, 200, 300, and 400
Old TF pier	Triaxial	0.6	Uniform pressure	400, 500, 600, and 800
National Cooperative Highway Research Program abutment	Plane strain	0.2	Footing pressure[a]	150, 250, and 300
Japanese abutment	Plane strain	1.4	Footing pressure[b]	118 and 137
Shored MSE wall	Plane strain	1.13	Footing pressure[c]	250, 285, and 320
French MSE wall	Plane strain	0.58	Footing pressure[d]	30 and 100
Royal Military College MSE wall	Plane strain	0.3	Uniform pressure	30, 60, and 90
New TF Piers 6, 9, 12, and 14	Triaxial	Not applicable	Uniform pressure	Varied

[a]Rectangular footing, 4.57×0.91 m.
[b]Rectangular footing, 4×2 m.
[c]Rectangular footing, 2.5×1.0 m.
[d]Strip footing, width $= 1.0$ m.

pier was 5.4 m and reinforced by woven PP geotextile (Amoco 2044) at a spacing of 0.2 m. The pier was 4.8 m in length and 3.6 m in width at the base, but the size decreased slightly towards the top. As the fabric was stronger in the cross-machine direction than in the machine direction, the reinforcement direction was alternated in the reinforced soil. According to Helwany et al. (2007), the stiffness in the cross-machine direction was about 1,200 kN/m at small strain. The stiffness in the machine direction was then estimated as 960 kN/m based on the differences in rupture strain and strength. The fill material was similar to that employed in the TF GRSC tests, according to their source location, dry unit weights, and parameters of particle size distributions. The soil parameters from triaxial tests in Wu et al. (2013) were therefore used in the research reported in this paper. Triaxial stress condition of soil was assumed because the same block facing was used on the four sides of the pier and the overall reinforcement stiffness was similar in the two directions. The soil deformations in the length and width directions of the pier were therefore not expected to be considerably different.

The loads in the reinforcement layer 0.6 m below the pier top were analyzed. This layer was selected as the measured values were

Table 3. Parameters of Soils

Reinforced soil mass or MSE wall	Soil as per the Unified Soil Classification System	Unit weight (kN/m^3)	ϕ (degrees)	$\Delta\phi$ (degrees)	c (kPa)	K	k	n	R_f
Turner-Fairbank GRSC I and II	GW-GM[a]	25	60	15.45	0	7.49	1,268	0.47	0.62
Old TF pier	GW-GM[b]	25	57	15.45	0	6.25	1,000	0.47	0.62
National Cooperative Highway Research Program abutment	SP-SM[c]	18.4	41	0	20	3	313	0.713	0.828
Japanese abutment	GW-GM[d]	19.7	53	0	0	4.17	2,132	0.52	0.838
Shored MSE wall	SP[e]	15.7	37	0	30	3	900	0.27	0.84
French MSE wall	SP[f]	19	40	0	4	3.85	170	0.42	0.88
Royal Military College MSE wall	SP[g]	16.67	44	0	2	3.69	1,150	0.5	0.86
New TF Piers 6, 9 12, and 14	GW-GM[h]	25	57 and 57.4	15.45 and 9.76	0	6.25	1,000	0.47	0.62

[a]Triaxial test data from Wu et al. (2013).
[b]Assumed to be the same as the soil of A.
[c]Triaixal test data from Helwany et al. (2007).
[d]Triaxial test data from Kohata et al. (1997).
[e]Triaxial test data from Lee (2010).
[f]Triaxial test data from Arab et al. (2001).
[g]Parameters from Hatami and Bathurst (2006).
[h]In Prediction 1, assumed to be the same the soil of A while in Prediction 2 the soil strength interpreted from the direct shear strength in Nicks et al. (2013).

reported in Wu et al. (2013). Besides, the influence of block facing was not considered in the research reported in this paper but it is expected to be small close to the pier top. The reinforcement loads under four levels of surcharge loadings were analyzed, as shown in Table 2.

National Cooperative Highway Research Program Abutment

This section discusses a National Cooperative Highway Research Program (NCHRP) abutment as per Wu et al. (2006a). The test abutment was 4.65 m in height and consisted of two sections, i.e., (1) reinforced with stronger PP geotextile (i.e., Amoco 2044), and (2) reinforced with a weaker PP geotextile (i.e., Mirafi 500X). The reinforcement spacing was mostly 0.2 m but intermediate layers were employed underneath the footings. In the research reported in this paper, the section reinforced with Mirafi 500X was analyzed since the measured strains in the other section were reported to be questionable according to Wu et al. (2006a) and Helwany et al. (2007). The analyzed reinforcement layer was 0.2 m below the footing and its maximum strains under three levels of footing pressure were calculated.

The abutment was 5.75-m wide and the wing wall also used the same concrete blocks. However, test results showed that the lateral movement of the wing wall was much smaller and Helwany et al. (2007) reported that assumption of plane-strain condition resulted in a similar response at the center of the abutment compared to that considering the three-dimensional (3D) boundary condition. Therefore, in the research reported in this paper, the plane-strain condition was assumed in the analysis of reinforcement load. The soil parameters were fitted from the triaxial test results reported in Helwany et al. (2007) but the friction angle was increased to consider the plane-strain condition (Georgiadis et al. 2004). The critical-state friction angle of the silty sand was assumed to be 30°, from which the stress dilatancy constant K was calculated. The reinforcement stiffness was based on the test result provided in Helwany et al. (2007).

Japanese Abutment

This section discusses a Japanese abutment as per Uchimura et al. (1996). The test abutment was constructed to investigate the effectiveness of preloading on geosynthetic reinforced soil but the research reported in this paper only focused on the preloading stage. The abutment was 5-m high and divided into three sections. It was reinforced by a polyvinyl alcohol (PVA) geogrid at a spacing of 0.3 m. The strains at two locations (E34 and E35) in the middle section (3M) under two levels of footing pressure were calculated by the proposed method and compared to the measured values. The vertical stresses at the two locations were obtained based on the Boussinesq solution.

The fill material was one type of well-graded gravel with silt, the triaxial stress-strain relationship of which at $\sigma_3 = 49$ kPa was reported in Kohata et al. (1997). The soil parameters were therefore determined based on this test but considering plane-strain improvement of friction angle, while the modulus exponent n was directly obtained from Kohata et al. (1997). The stress dilatancy constant K was determined using Eq. (3a) based on the ratio of $\Delta\varepsilon_3/\Delta\varepsilon_1$ at small deviatoric stress in Kohata et al. (1997). The reinforcement stiffness was based on the tensile test on the same geogrid reported in Kongkitkul et al. (2007).

Shored MSE Wall

This section discusses a shored MSE wall as per Morrison et al. (2006). The full-scale test was carried out to study the application of shored MSE wall for road embankment widening. It consisted of two sections, in one of which the reinforcement was connected to the shoring wall. The wall was 5.5-m high, backfilled with one type of poorly graded sand, and reinforced by uniaxial high-density polyethylene (HDPE) geogrid. The reinforcement stiffness was reported to be 1,300 kN/m in Morrison et al. (2006) and the reinforcement spacing was mainly 0.46 m, but was reduced by half close to the top. The reinforcement length ranged from 1.4 m at the base to 2.1 m close to the top. The rectangle footing was 1.0 m in width and was 0.79 m away from the wire-welded facing.

The maximum reinforcement strains in a reinforcement layer 1.13 m below the footing in the unconnected section were calculated by the proposed method. The connection to the shoring wall reduced the maximum reinforcement strain but the boundary condition is not considered in the proposed method. The triaxial test data of soil were reported in Lee (2010), from which the soil parameters were determined considering plane-strain increase of friction

angle. The dilatancy constant K was determined assuming critical-state friction angle of 30°. The vertical stresses below the center of footing were calculated by the Boussinesq method.

French MSE Wall

This section discusses a French MSE wall as per Arab et al. (2001). The wall was 4.35-m high, backfilled with one type of poorly graded sand, and reinforced by woven geotextile at varying but large spacing. Another test using nonwoven geotextile was also reported in Arab et al. (2001), but the reinforcement was too weak and large strain was mobilized in the reinforced soil under a small footing load. The MSE wall included a modular-block facing with a batter angle and in order to minimize the influence of the inclined facing, only the maximum strains in a reinforcement layer 0.58 m below the footing were analyzed for two levels of footing pressure.

The soil parameters were determined by using the triaxial test data in Arab et al. (2001) and as usual the friction angle was increased to consider the plane-strain condition. The dilatancy constant K was calculated by using the peak friction angle and dilatancy angle reported in Arab et al. (2001). The reinforcement stiffness was interpreted from the tensile test result in the same reference.

Royal Military College MSE Wall

This section discusses a Royal Military College (RMC) MSE wall as per Walters (2004). The test was carried out at the Royal Military College in Canada. A series of tests with different reinforcements, reinforcement spacings, or facing elements were conducted, but considering the boundary condition assumed in the proposed method, only the MSE wall reinforced by a welded wire mesh (WWM) and having a wrapped around facing was analyzed in the research reported in this paper. The wall was 3.6 m in height, backfilled by one type of poorly graded sand, and having a reinforcement spacing of 0.6 m. The wall facing had a batter angle of 8° and in order to minimize the influence of inclined facing, only the maximum strains in the top reinforcement layer under three levels of surcharge pressure were analyzed by the proposed method.

The soil parameters (except the dilatancy constant K) were reported in Hatami and Bathurst (2006). The value of K was determined by the peak friction angle and dilatancy angle (Hatami and Bathurst 2006). The reinforcement stiffness was 3,100 kN/m according to Walters (2004).

New TF Piers

This section discusses new TF piers as per Nicks et al. (2013). Recently, a series of large scale tests were carried out on miniature reinforced soil piers at the TFHRC to gain insights into the reinforcement load and deformation property of a reinforced soil mass. The tests investigated the effects of different fill materials, different values of reinforcement stiffness, and different reinforcement spacings. The influence of modular block facing was also studied. In the research reported in this paper, considering the availability of soil data, only the tests backfilled by well-graded gravel (i.e., GW-GM) were analyzed. Furthermore, the tests without modular block facing resulted in much larger deformation under the same surcharge, which was due to the negligible soil confinement at the sides. The soil at the sides failed and spalled first under compression deformation, which then propagated towards the core of the reinforced soil mass. This boundary condition was not considered in the proposed method; hence only four tests with modular block facing were modeled in the research reported in this paper.

Triaxial test results of the fill material were not available but direct shear test results were provided in Nicks et al. (2013). The particle size distribution of the fill was not very different from that in Wu et al. (2013) and the material source and compacted dry density were also similar. Accordingly, the stiffness and dilatancy parameters were assumed to be the same as those obtained from the triaxial tests in Wu et al. (2013). The triaxial stress condition was assumed in this series of tests, similar to that for the old TF pier (Wu et al. 2001). Two sets of soil strength were employed in the compression predictions. These two predictions are, as follows: (1) the same as that for the TF GRSC composites, and (2) based on the direct shear test results. The triaxial friction angle was derived from the relationships among triaxial, plane-strain, and direct shear strengths of sandy soil (Lade and Lee 1976; Allen et al. 2004). The minipiers were all reinforced by woven PP geotextile, but with different values of stiffness or reinforcement spacing, as shown in Table 1. The values of reinforcement stiffness in the four tests were interpreted from the geosynthetic specifications (Nicks et al. 2013). However, the values may be underestimated at small reinforcement strain as they were mostly interpreted based on the load at 5% strain.

According to Nicks et al. (2013), strains were also measured in some of the reinforcement layers but the results were not available at the time of the research reported in this paper. Therefore, only the compressions of the reinforced soil masses were predicted.

Results

Prediction of Reinforcement Load under Surcharge Loading

Fig. 1 shows the comparison between the predicted and measured reinforcement strains for eight large-scale tests of reinforced soil masses or MSE walls. The proposed method was capable of analyzing reinforcement load when the reinforced soil deformation was modest, which is generally the case for reinforced soil structures under a service loading condition.

Prediction of Compression of Reinforced Soil Mass

The compression of GRSC I and II reported in Wu et al. (2013) was employed to validate the proposed method of compression analysis. In this case, the actual measured reinforcement strains were employed to back-calculate the values of virtual reinforcement stiffness in the reinforced soil mass. That is to say, the reinforcement layer with the largest measured strain was assigned the actual value

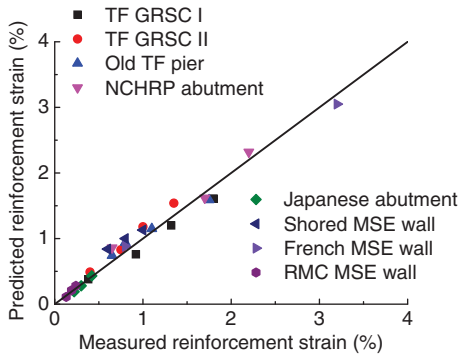

Fig. 1. Comparison of predicted and measured reinforcement strains in large-scale tests

J. Geotech. Geoenviron. Eng., 2015, 141(6): 04015017

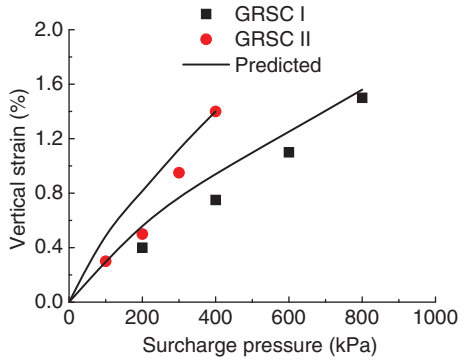

Fig. 2. Comparison of reinforced soil compression from the analytical method and large-scale tests

as shown in Table 1, while those of the other layers were assigned stiffness values according to Eq. (13). Fig. 2 shows the comparison of average compression strains from the tests and analyses. Except at one level of surcharge pressure, the proposed method can reproduce the compression of reinforced soil mass satisfactorily. Overall the prediction was conservative to some extent at low surcharge pressure. The compression strain of GRSC II under a surcharge pressure of 200 kPa was abnormally small in the test. It was very close that of GRSC I, even though the reinforcement spacing was doubled.

The predictions of the average vertical strains in the minipiers (Nicks et al. 2013) are shown in Fig. 3 together with the measured values. In these cases, the empirical distribution of reinforcement strain by Elton and Patawaran (2004) was used. The predictions were conducted using two sets of soil strength, as discussed previously. Overall the predicted compressions were somewhat larger than the measured values but the difference was acceptable except for TF 12. Prediction 2 employing the interpreted soil strength from the direct shear tests was slightly larger than Prediction 1. For TF 12, the test resulted in very small compression strain at low surcharge pressure, which is quite different from the other tests. This cannot be explained by the difference in reinforcement stiffness and reinforcement spacing. Comparing TF 12 and 6, the global reinforcement stiffness $\sum J_i/H$ (Allen et al. 2004), where J_i is the reinforcement stiffness of the ith layer, and H is the height of reinforced soil mass, was actually smaller for TF 12 but the compression strain was much smaller at low surcharge pressures. Rather, the difference in soil compaction might have contributed to the very small compression strain at low pressure in this test.

Figs. 2 and 3 show that the model overall overpredicted the vertical strain under low surcharge pressure. This can mostly be explained by the neglecting of the compaction effect. The locked-in lateral soil stress in the tests resulted in larger soil stiffness and therefore smaller compression than the predictions by the proposed method. Another possible contribution to this difference is the facing blocks of the TF piers, which have helped to stabilize the reinforced soil piers but were not considered in the proposed method.

Parametric Study

A parametric study was carried out to investigate the influences of soil dilatancy and soil nonlinearity under operational surcharge loading. To this end, the reinforced soil mass TF GRSC I and its parameters (Wu et al. 2013) were employed as the base case. The influence of soil dilatancy was firstly analyzed, in which the Rowe (1962) constant K was calculated as $K = (1 + \sin\phi)(1 - \sin\psi)/[(1 - \sin\phi)(1 + \sin\psi)]$. The angle of dilatancy ψ was varied from 0 to 25°, while the angle of internal friction was kept constant. As shown in Fig. 4(a), although its influence on the reinforcement strain at low surcharge loading was negligible, its effect on the compression strain was more obvious. The influences on the reinforcement strain and compression strain increased with an increase in the surcharge loading, as shown in Fig. 4(a). With the same angle of internal friction and stiffness, an increase in the dilatancy angle led to an increase in the lateral soil strain under the same

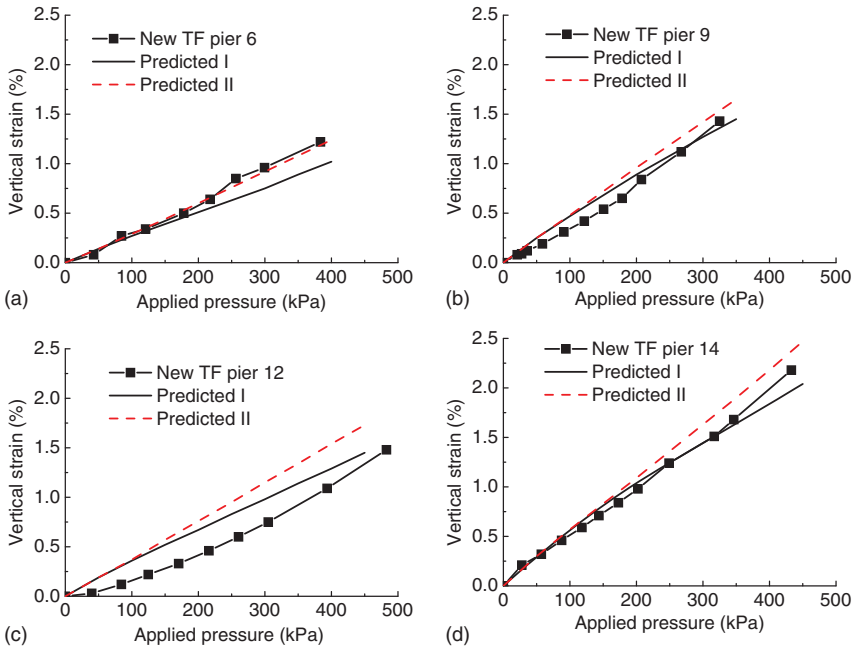

Fig. 3. Prediction of the compressions of four minipiers under surcharge loading: (a) new TF Pier 6; (b) new TF Pier 9; (c) new TF Pier 12; (d) new TF Pier 14

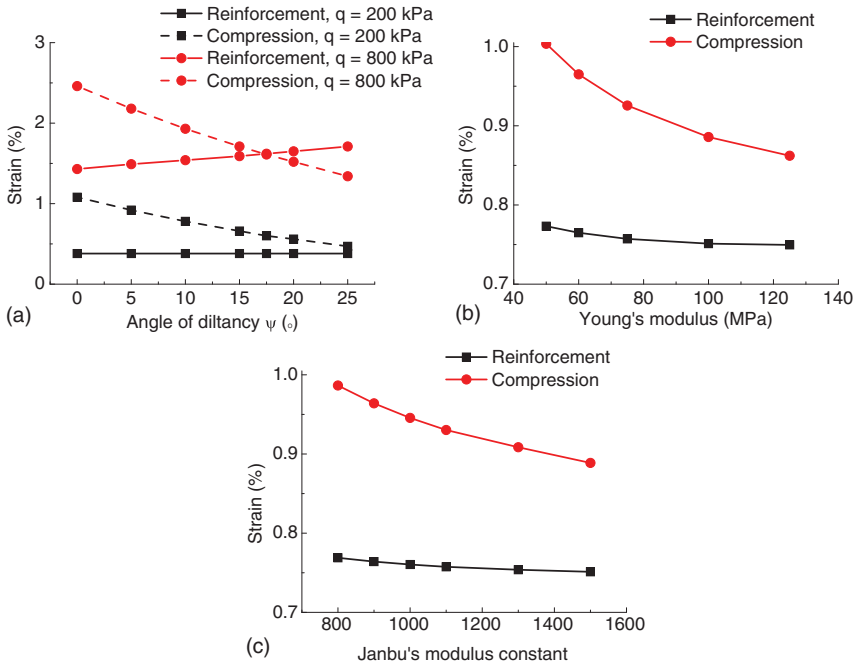

Fig. 4. Results of parametric study: (a) influence of the angle of dilatancy; (b) influence of soil modulus assuming linear elastic behavior; (c) influence of soil modulus number assuming pressure-dependent soil behavior

vertical stress, which resulted in an increase in the reinforcement load.

There exist two levels of nonlinearity in the stress-strain relationship of soil, as follows: (1) the dependence of stiffness on confining pressure, and (2) its dependence on shear strain. The soil modulus was first assumed to be a constant, and the maximum reinforcement strain and the average compression strain were analyzed under a surcharge loading of 400 kPa. The relationship between lateral and vertical soil strain still was in accordance with Eq. (8*a*), which indicated a nonconstant Poisson's ratio if it is converted into linear elastic stress-strain relationship. Fig. 4(b) shows the changes of strains with the soil modulus. A modulus around 60 MPa resulted in strain values similar to those of the base case but for a problem like this it would be difficult to estimate a proper constant modulus as the confining pressure in the reinforced soil is not known in advance. On the other hand, if the soil modulus was assumed to be dependent on the confining pressure in accordance with the Janbu (1963) equation $E = E_0 p_a(\sigma_l/p_a)^n$, where E_0 is the Janbu's modulus constant, and $n = 0.47$ for this soil (Janbu 1963), the analyzed maximum reinforcement strain and average soil strain were close to those of the base case when E_0 was about 950, as shown in Fig. 4(c). This value approximately corresponds to the modulus of soil at about 1% vertical strain in plane-strain compression. Between the two strains, the average compression strain was more sensitive to the modulus value, as shown in Figs. 4(b and c).

The parametric study indicates that nonlinear elasticity may be applicable to analyze the behavior of reinforced soil mass when the surcharge loading was low and the soil strain was small. But the dependence of modulus on the confining pressure together with a nonconstant Poisson's ratio (Janbu 1963; Duncan et al. 1980) are both necessary to obtain reliable results.

Discussion

The proposed method has the potential to predict reinforcement load and compression of reinforced soil mass under surcharge loading. However, there are some issues that deserve attention in its application.

The surcharge loads on most of the reinforced soil masses or MSE walls were applied by rigid slabs or footings, which might have contributed to some of the discrepancy in the measured and predicted results. It is well-accepted that rigid footing leads to a nonuniform surcharge pressure. Particularly, if uniform compression is applied to a reinforced soil mass without facing, like those in Nicks et al. (2013), the vertical stress shall be larger at the center, while the soil close to the sides shall fail first, and the failure shall then propagate towards the core.

The facing element of the reinforced soil mass helps to stabilize the reinforced soil. Its effect can be taken into account by the initial lateral stress σ_{l0} in Eq. (5). Unfortunately, the value is related to many factors including the facing type, facing base restriction, stress level, soil-facing interaction, and reinforcement facing connection (Wu 2007; Leshchinsky and Vahedifard 2012; Huang et al. 2010; Ehrlich and Mirmoradi 2013), and the state of knowledge at present is still not adequate for its quantification.

Another issue is the reinforcement stiffness. It is well-known that geosynthetic reinforcement exhibits rate-dependent behavior under loading (Shinoda and Bathurst 2004; Kongkitkul et al. 2007; Liu et al. 2009; Liu and Won 2009). The stiffness at a small loading rate is smaller. In the research reported in this paper, the values of the reinforcement stiffness were all obtained from standard tension tests. The test condition may be close to the condition in the reinforced soil mass during surcharge loading. However, after surcharge loading the reinforced soil mass shall undergo creep deformation and the isochrones of geosynthetic reinforcements should be used to estimate the reinforcement stiffness (Hatami and Bathurst 2006; Liu and Won 2014). Most geosynthetic reinforcements also exhibit a nonlinear stress-strain relationship, which can be taken into account by the proposed method for reinforcement load (Liu and Won 2014).

Still another issue is the assumed distribution of reinforcement strains along the height of reinforced soil, which should be

determined from extensive large-scale tests. The stress state of soil in the tests by Elton and Patawaran (2004) was only triaxial and the number of tests may not be large enough. Nonetheless, any distribution can be easily applied together with the proposed method.

The last issue is the compaction effect, which is not considered in the proposed method. As discussed in Bathurst et al. (2009) and Liu and Won (2014), the compaction effect on the reinforcement load shall be erased when the surcharge pressure is larger than the equivalent compaction pressure. However, soil compaction still affects the compression strain of the reinforced soil mass, which may be the main reason why overall the proposed method overestimated the compression strains at low pressures. If the equivalent compaction pressure can be quantified, the overprediction can be alleviated by considering elastic unloading and reloading at small pressure. The approach introduced in Liu and Won (2014) can be slightly revised for this purpose. What is difficult at present is the quantification of the equivalent pressure, as explained in Liu and Won (2014). The dynamic contact pressure from the compaction device cannot be directly applied in the research reported in this paper, as it is far too conservative according to Bathurst et al. (2009). Owing to this difficulty, this is not done in the research reported in this paper.

Conclusions

The analytical method in Liu and Won (2014) was extended to calculate the reinforcement load and compression of reinforced soil mass under surcharge loading. The new features of the extension consist of the consideration of triaxial stress state, the analysis of vertical soil strain under surcharge loading, and an approximate methodology to take into account end restriction on the compression of reinforced soil mass. In addition, the method for reinforcement load was evaluated using eight large-scale tests of reinforced soil mass or MSE walls, and the method for reinforced soil compression was validated against two large-scale tests of reinforced soil composite. The method was finally applied to predict the compressions of four reinforced soil minipiers under surcharge loading. The paper shows that the proposed method has the capacity to unify the analyses of reinforcement load and compression of a reinforced soil mass under surcharge loading, provided that the soil has not or just reached the peak shear strength.

At this stage, the proposed method still has three limitations, including (1) the neglecting of compaction effect, (2) the neglecting of facing restriction, and (3) the assumed distribution of reinforcement strains over height. Limitation 1 can be alleviated by considering the elastic unloading and reloading according to Liu and Won (2014) when the surcharge pressure was smaller than the equivalent compaction pressure. Limitation 2 can be reduced by incorporating the influence of additional lateral soil stress σ_{l0}. Limitation 3 can be eliminated when more measured strain distributions from large-scale tests become available. However, the available knowledge at present prevents the determination of the equivalent compaction pressure and the additional lateral soil stress. Further study in these areas is necessary.

The proposed method can be employed to analyze reinforcement load and compression strain of reinforced soil mass under low to medium surcharge loading before the soil strength is fully mobilized. When the surcharge was low and the soil strain was small, the dependence of soil stiffness on soil strain may be neglected, and the Janbu (1963) equation may be employed together with a nonconstant Poisson's ratio to estimate these two responses using theory of elasticity (Duncan et al. 1980; Hoffman and Wu 2014).

Acknowledgments

The research reported in this paper was supported by the National Natural Science Foundation of China (Grant No. 51379082). The financial support is gratefully acknowledged.

References

Abramento, M., and Whittle, A. J. (1993). "Shear-lag analysis of planar soil reinforcement in plane-strain compression." *J. Eng. Mech.*, 10.1061/(ASCE)0733-9399(1993)119:2(270), 270–291.

Abu-Hejleh, N., Zornberg, J. G., Wang, T., and Watcharamonthein, J. (2002). "Monitored displacements of unique geosynthetic-reinforced soil bridge abutments." *Geosynthet. Int.*, 9(1), 71–95.

Adams, M. T., Lillis, C. P., Wu, J. T. H., and Ketchart, K. (2002). "Vegas mini pier experiment and postulate of zero volume change." *Proc., SeventhInt. Conf. on Geosynthetics*, Swets & Zeitlinger, Lisse, Netherlands, 389–394.

Adams, M. T., Nicks, J., Stabile, T., Wu, J. T. H., Schlatter, W., and Hartmann, J. (2011). "Geosynthetic reinforced soil integrated bridge system: Synthesis report." *Rep. No. Federal Highway Administration (FHWA)-HRT-11-027*, Washington, DC.

Adams, M. T., Schlatter, W., and Stabile, T. (2007). "Geosynthetic reinforced soil integrated abutments at the Bowman Road Bridge in Defiance County, Ohio." *Proc., Geo-Denver 2007*, ASCE, Reston, VA.

Allen, T. M., Bathurst, R. J., Holtz, R. D., Lee, W. F., and Walters, D. L. (2004). "New method for prediction of loads in steel reinforced soil walls." *J. Geotech. Geoenviron. Eng.*, 10.1061/(ASCE)1090-0241(2004)130:11(1109), 1109–1120.

Arab, R., Villard, P., and Gourc, J. P. (2001). "Use of reinforced soil bearing structures." *Ground Improv.*, 5(4), 163–175.

Bathurst, R. J., et al. (2009). "Influence of reinforcement stiffness and compaction on the performance of four geosynthetic-reinforced soil walls." *Geosynthet. Int.*, 16(1), 43–59.

Bathurst, R. J., Miyata, Y., Nernheim, A., and Allen, A. M. (2008). "Refinement of K-stiffness method for geosynthetic reinforced soil walls." *Geosynthet. Int.*, 15(4), 269–295.

Berg, R. R., Christopher, B. R., and Samtani, N. C. (2009). "Design of mechanically stabilized earth walls and reinforced slopes." *Rep. No. Federal Highway Administration (FHWA)-NHI-10-024 Vol I and NHI-10-025 Vol II*, Washington, DC.

Duncan, J. M., Byrne, P., Wong, K. S., and Mabry, P. (1980). "Strength, stress strain and bulk modulus parameters for finite element analyses of stresses and movements in soil masses." *Geotechnical Engineering Research Rep. No. Univ. of California Berkeley (UCB)/GT/80-O1*, Berkeley, CA.

Ehrlich, M., and Mirmoradi, S. H. (2013). "Evaluation of the effects of facing stiffness and toe resistance on the behavior of GRS walls." *Geotext. Geomembr.*, 40, 28–36.

Ehrlich, M., Mirmoradi, S. H., and Saramago, R. P. (2012). "Evaluation of the effect of compaction on the behavior of geosynthetic-reinforced soil walls." *J. Geotext. Geomembr.*, 34, 108–115.

Ehrlich, M., and Mitchell, J. K. (1994). "Working stress design method for reinforced soil walls." *J. Geotech. Eng.*, 10.1061/(ASCE)0733-9410(1994)120:4(625), 625–645.

Elton, D. J., and Patawaran, M. A. B. (2004). "Mechanically stabilized earth reinforcement tensile strength from tests of geotextile-reinforced soil." *Transportation Research Record 1868*, Transportation Research Board, Washington, DC, 81–88.

Georgiadis, K., Potts, D. M., and Zdravkovic, L. (2004). "Modelling the shear strength of soils in the general stress space." *Comput. Geotech.*, 31(5), 357–364.

Hatami, K., and Bathurst, R. J. (2006). "Numerical model for reinforced soil segmental walls under surcharge loading." *J. Geotech. Geoenviron. Eng.*, 10.1061/(ASCE)1090-0241(2006)132:6(673), 673–684.

Helwany, S. M. B., Wu, J. T. H., and Kitsabunnarat, A. (2007). "Simulating the behavior of GRS bridge abutments." *J. Geotech. Geoenviron. Eng.*, 10.1061/(ASCE)1090-0241(2007)133:10(1229), 1229–1240.

Hoffman, P., and Wu, J. T. H. (2014). "An analytical model for predicting load–deformation behavior of the FHWA GRS-IBS performance test." *Int. J. Geotech. Eng.*, in press.

Huang, B., Bathurst, R. J., Hatami, K., and Allen, T. M. (2010). "Influence of toe restraint on reinforced soil segmental walls." *Can. Geotech. J.*, 47(8), 885–904.

Janbu, N. (1963). "Soil compressibility as determined by oedometer and triaxial tests." *Proc., European Conf. on Soil Mech. and Foundation Eng.*, Vol. 1, International Society of Soil Mechanics and Foundation Engineering (ISSMFE), London, 19–25.

Juran, I., and Chen, C. L. (1989). "Strain compatibility design method for reinforced earth walls." *J. Geotech. Eng.*, 10.1061/(ASCE)0733-9410(1989)115:4(435), 435–456.

Juran, I., Ider, H. M., and Farrag, K. (1990). "Strain compatibility analysis for geosynthetics reinforced soil walls." *J. Geotech. Eng.*, 10.1061/(ASCE)0733-9410(1990)116:2(312), 312–329.

Kohata, Y., Tatsuoka, F., Wang, L., Jiang, G. J., Hoque, E., and Kodaka, T. (1997). "Modelling the non-linear deformation properties of stiff geomaterials." *Geotechnique*, 47(3), 563–580.

Kongkitkul, W., Hirakawa, D., Tatsuoka, F., and Kanemaru, D. (2007). "Effects of geosynthetic reinforcement type on the strength and stiffness of reinforced sand in plane strain compression." *Soils Found.*, 47(6), 1109–1122.

Lade, P. V., and Lee, K. L. (1976). "Engineering properties of soils." *Rep. No. Univ. of California Los Angeles (UCLA)-ENG-7652*, Los Angeles.

Lee, Y. B. (2010). "Deformation behavior of shored mechanically stabilized earth (SMSE) wall systems." Ph.D. thesis, Univ. Colorado, Boulder, CO.

Leshchinsky, D., and Boedeker, R. H. (1989). "Geosynthetic reinforced soil structures." *J. Geotech. Eng.*, 10.1061/(ASCE)0733-9410(1989)115:10(1459), 1459–1478.

Leshchinsky, D., and Vahedifard, F. (2012). "Impact of toe resistance in reinforced masonry block walls: Design dilemma." *J. Geotech. Geoenviron. Eng.*, 10.1061/(ASCE)GT.1943-5606.0000579, 236–240.

Liu, H., Wang, X., and Song, E. (2009). "Long-term behavior of GRS retaining walls with marginal backfill soils." *J. Geotext. Geomembr.*, 27(4), 295–307.

Liu, H., and Won, M. S. (2009). "Long-term reinforcement load of geosynthetic reinforced soil retaining walls." *J. Geotech. Geoenviron. Eng.*, 10.1061/(ASCE)GT.1943-5606.0000052, 875–889.

Liu, H., and Won, M. S. (2014). "Stress dilatancy and reinforcement load of vertical-reinforced soil composite: Analytical method." *J. Eng. Mech.*, 10.1061/(ASCE)EM.1943-7889.0000686, 630–639.

Morrison, K. F., Harrison, F. E., Collin, J. G., Dodds, A., and Arndt, B. (2006). "Shored mechanically stabilized earth (SMSE) wall systems, design guidelines." *Rep. Federal Highway Administration (FHWA)-CFL/TD-06-001*, Washington, DC.

Nicks, J. E., Adams, M. T., Ooi, P. S. K., and Stabile, T. (2013). "Geosynthetic reinforced soil performance testing—Axial load deformation relationships." *Rep. Federal Highway Administration (FHWA)-HRT-13-066*, Washington, DC.

Rowe, P. W. (1962). "The stress–dilatancy relation for static equilibrium of an assembly of particles in contact." *Proc. Roy. Soc. London Ser. A*, 269(1339), 500–527.

Shinoda, M., and Bathurst, R. J. (2004). "Lateral and axial deformation of PP, HDPE and PET geogrids under tensile load." *Geotext. Geomembr.*, 22(4), 205–222.

Uchimura, T., Tateyama, M., Tanaka, I., and Tatsuoka, F. (2003). "Performance of a preloaded-prestressed geogrid-reinforced soil pier for a railway bridge." *Soil. Foundations*, 43(6), 155–171.

Uchimura, T., Tatsuoka, F., Sato, T., Tateyama, M., and Tamura, M. (1996). "Performance of preloaded and prestressed geosynthetic-reinforced soil." *Earth reinforcement*, H. Ochiai, K. Omine, and N. Yasufuku, eds., Balkema, Rotterdam, Netherlands, 537–542.

Walters, D. L. (2004). "Behavior of reinforced soil retaining walls under uniform surcharge loading." Ph.D. thesis, Queen's Univ., Kingston, ON, Canada.

Wood, D. (1990). *Soil behaviour and critical state soil mechanics*, Cambridge University Press, Cambridge, U.K.

Wu, J. T. H. (2007). "Lateral earth pressure against the facing of segmental GRS walls." *Geosynthetics in Reinforcement and Hydraulic Applications, Geo-Denver 2007*, ASCE, Reston, VA, 1–11.

Wu, J. T. H., Ketchart, K., and Adams, M. (2001). "GRS bridge piers and abutments." *Rep. Federal Highway Administration (FHWA)-RD-00-038*, Washington, DC.

Wu, J. T. H., Lee, K. Z. Z., Helwany, S. B., and Ketchart, K. (2006a). "Design and construction guidelines for GRS bridge abutment with a flexible facing." *National Cooperative Highway Research Program (NCHRP) Rep. 556*, Washington, DC.

Wu, J. T. H., Lee, K. Z. Z., and Pham, T. (2006b). "Allowable bearing pressures of bridge sills on GRS abutments with flexible facing." *J. Geotech. Geoenviron. Eng.*, 10.1061/(ASCE)1090-0241(2006)132:7(830), 830–841.

Wu, J. T. H., Pham, T. Q., and Adams, M. T. (2013). "Composite behavior of geosynthetic reinforced soil mass." *Rep. Federal Highway Administration (FHWA)-HRT-10-077*, Washington, DC.

Wu, J. T. H., Yang, K. H., Mohamed, S., Pham, T., and Chen, R. H. (2014). "Suppression of soil dilation–A reinforcing mechanism of soil-geosynthetic composites." *Transp. Infrastruct. Geotechnol.*, 1(1), 68–82.